Biophysical Journal
Article

Biophysical Society

On multistability and constitutive relations of cell motion on fibronectin lanes

Behnam Amiri,[1] Johannes C. J. Heyn,[2] Christoph Schreiber,[2] Joachim O. Rädler,[2,*] and Martin Falcke[1,3,*]
[1]Max Delbrück Center for Molecular Medicine in the Helmholtz Association, Berlin, Germany; [2]Fakultät für Physik, Ludwig-Maximilians-Universität München (LMU), Munich, Germany; and [3]Department of Physics, Humboldt University, Berlin, Germany

ABSTRACT Cell motility on flat substrates exhibits coexisting steady and oscillatory morphodynamics, the biphasic adhesion-velocity relation, and the universal correlation between speed and persistence (UCSP) as simultaneous observations common to many cell types. Their universality and concurrency suggest a unifying mechanism causing all three of them. Stick-slip models for cells on one-dimensional lanes suggest multistability to arise from the nonlinear friction of retrograde flow. This study suggests a mechanical mechanism controlled by integrin signaling on the basis of a biophysical model and analysis of trajectories of MDA-MB-231 cells on fibronectin lanes, which additionally explains the constitutive relations. The experiments exhibit cells with steady or oscillatory morphodynamics and either spread or moving with spontaneous transitions between the dynamic regimes, spread and moving, and spontaneous direction reversals. Our biophysical model is based on the force balance at the protrusion edge, the noisy clutch of retrograde flow, and a response function of friction and membrane drag to integrin signaling. The theory reproduces the experimentally observed cell states, characteristics of oscillations, and state probabilities. Analysis of experiments with the biophysical model establishes a stick-slip oscillation mechanism, and explains multistability of cell states and the statistics of state transitions. It suggests protrusion competition to cause direction reversal events, the statistics of which explain the UCSP. The effect of integrin signaling on drag and friction explains the adhesion-velocity relation and cell behavior at fibronectin density steps. The dynamics of our mechanism are nonlinear flow mechanics driven by F-actin polymerization and shaped by the noisy clutch of retrograde flow friction, protrusion competition via membrane tension, and drag forces. Integrin signaling controls the parameters of the mechanical system.

SIGNIFICANCE Biophysical comprehension of cell motion and morphodynamics means to characterize them experimentally and explain them based on the internal cell dynamics. We characterize motion of MDA-MB-231 cells by analyzing 29,500 trajectories on one-dimensional fibronectin lanes. We suggest the intrinsic dynamics to derive from three constituents, namely the protrusion edge force balance, the noisy clutch mechanism of retrograde flow, and integrin signaling. Corresponding theory reproduces the measured morphodynamics. It also captures the measured motion characteristics given as the constitutive adhesion-velocity relation and persistence-speed relation and its response to drugs. We predict the constitutive force-velocity relation. Hence, the constituents of the mechanism, which apply to many cell types, explain the complex morphodynamics and constitutive motion relations.

INTRODUCTION

The motion of eukaryotic cells is essential for embryonic development, wound healing, immune responses, and tumor metastasis (1). Much effort has been devoted to the study of mesenchymal migration with prototypical in vitro motion of cells on two-dimensional (2D) adhesive substrates. Cell migration starts with polarization breaking the spatial symmetry and the formation of a lamellipodium, which is a protrusion of a thin sheet of cytoplasm (0.1–0.3 μm thick) covering tens to hundreds of square micrometers (2–7). The lamellipodium is mechanically stabilized by adhesion with the substrate (8–14) and is constructed from a network of actin filaments (15–19). Polymerization of filament barbed ends at the leading edge of the lamellipodium generates motion and pushes the edge forward (20–23). Further back, the pointed ends depolymerize and replenish the pool of actin monomers (18,19). Once cells are moving, their shape is

Submitted October 21, 2022, and accepted for publication January 31, 2023.

*Correspondence: raedler@lmu.de or martin.falcke@mdc-berlin.de

Editor: Dimitrios Vavylonis.

https://doi.org/10.1016/j.bpj.2023.02.001

determined by internal force-generation patterns and adhesion (24–29).

Many cell types obey both the adhesion-velocity relation and the universal correlation between speed and persistence (UCSP). The dependency of the cell velocity on adhesion exhibits a velocity maximum at intermediate strength, and slower velocities both at weak and strong adhesion (10–14,26,30–35). Results on the UCSP, describing the relation between cell velocity and persistence time, suggest it to be of similar universality (36). The faster cells move, the more persistent they move. Maiuri et al. report this observation for many different cell types and suggest persistence time to depend exponentially on cell velocity (36). These types of relations describing the response of a system to external parameters are called constitutive relations in the fields of physics and engineering. The stationary force-velocity relation is another constitutive relation we will discuss.

Another general observation is that both the shape and the motile state of cells are highly dynamic. Cells stop and start to move again, develop new protrusions, and change direction (25,29,37–53). In addition to these states of motion, there exist states distinguished by the dynamic regime of front protrusion and cell back and/or back protrusion. Stationary and oscillatory dynamic regimes with one or several protrusions have been observed and have caused a surge of interest in multistability in cell motility (5,47,51,52,54–62).

Multistability with its state dynamics, biphasic adhesion-velocity relation, and the UCSP appear to describe the motile behavior of many different cell types. Mechanisms have been suggested for multistability (47,56,57,59–62), the biphasic adhesion-velocity relation (11,31,34,35), the UCSP (36), and the stationary force-velocity relation (63), each separately. However, the generality and concurrency of multistability and the constitutive relations strongly suggest that a single mechanism should explain all three of them.

In search for such a mechanism, we carry out a series of experiments with MDA-MB-231 cells on one-dimensional (1D) lanes in a range of fibronectin concentrations and formulate our suggestion for a mechanism as a biophysical model based on previous studies (35,64). The mechanism involves the force balance at the protrusion edges, the clutch mechanism of retrograde flow, competing protrusions, and integrin signaling. Our key finding is that the intracellular dynamics generating multistability also determine the constitutive relations. We introduce basic experimental observations in the section "dynamic cell states," characterize cell states and compare experimental and simulated data in "analysis of dynamic cell states," and explain state transitions and their relation to the UCSP in "transitions between cell states." We explain the ideas defining the theory and compute the force-velocity relation and adhesion-velocity relation in materials and methods.

MATERIALS AND METHODS

Cell culture

We cultured MDA-MB-231 breast cancer cells stably transduced with histone-2B mCherry (gift from Timo Betz, WWU Münster, Germany) in L15 medium with 2 mM Glutamax (Thermo Fisher Scientific, Waltham, MA, USA) plus 10% fetal bovine serum (Thermo Fisher) at 37°C. Cells were passaged every 2–3 days using Accutase (Thermo Fisher). For experiments, about 5000 cells were seeded per dish. After 2–3 h, cells adhered to the micropatterns and we exchanged the medium to L15 medium without phenol red. We then transferred the samples to the microscope and started measurements within 1–2 h. For inhibitor experiments 10 μM (+/−)-blebbistatin (Cayman Chemical, Ann Arbor, MI, USA), 100 nM latrunculin A (Merck, Darmstadt, Germany), or 0.25 nM calyculin A (Thermo Fisher) were added 2 h before the start of the experiment. As control we used dimethyl sulfoxide (Life Technologies, Darmstadt, Germany) equal to the amount used for the dilution of the inhibitors.

Micropatterning

Lanes (15 μm wide) which were homogeneously coated with fibronectin (FN) (YO Proteins, Ronninge, Sweden) were applied on an imaging dish with a polymer coverslip bottom (ibidi, Gräfelfing, Germany) using a microcontact printing protocol. The production of the polydimethylsiloxane stamps and the subsequent printing has been described previously (65). For all experiments, a range of FN densities was covered.

Determination of fibronectin densities

We determined the FN density via fluorescence intensity as described previously by our group (35). Lyophilized FN batches were resuspended and conjugated with Alexa Fluor 647 NHS ester (Thermo Fisher). We measured the concentration of FN in solution by optical absorption at 280 nm (Nanodrop, Thermo Fisher). The calibration factor that enables the conversion of fluorescence intensity to FN density was determined using microfluidic channel slides that were filled with an FN solution of known concentration.

Microscopy

We performed time-lapse imaging on an inverted fluorescence microscope (Nikon Eclipse Ti, Nikon, Tokyo, Japan) equipped with an XY-motorized stage, Perfect Focus System (Nikon), and a heating chamber (Okolab, Pozzuoli, Italy) set to 37°C. Arrays of fields of view were sequentially scanned and imaged using the motorized stage, the Perfect Focus System, a 10× CFI Plan Fluor DL objective (Nikon), a CMOS camera (PCO edge 4.2, Excelitas PCO, Kelheim, Germany) and the acquisition software NIS Elements (Nikon). Before the start of the time-lapse measurement, epifluorescence images of the FN patterns were taken. Phase-contrast images of the cells and epifluorescence images of their nuclei were then taken for 48 h at 10-min or 30-s intervals as indicated. Intervals of 10 min allowed scanning of $12 \times 12 = 144$ fields of view, while intervals of 30 s allowed $4 \times 4 = 16$ fields of view.

Image analysis

Image analysis was performed using a combination of MATLAB R2020a (MathWorks, Natick, MA, USA) scripts and FIJI (ImageJ) macros, based on previous work (35). FN lanes are detected using a Hough transformation of the fluorescence signal of the labeled FN. The position of the nuclei is tracked by setting a threshold after applying a background correction and band-pass filter to the fluorescent images of the nuclei. The coordinates of the nuclei are converted such that the x coordinates are parallel to the FN lanes. The position of the front and back of the cells is determined

via kymographs that are created along the center of the FN lane. The cell edge is then manually segmented. Code used to generate results in the current study is available on GitHub: https://github.com/behnam89amiri/Multistability_and_constitutive_relations_of_cell_motion.

Biophysical model

We define here the model constituents and their rate laws. This will result in differential equations for the protrusion lengths $L_{f,b}$ and friction coefficients $\kappa_{f,b}$ for the front (f) and back (b) protrusions. Protrusion edge velocities $v_{f,b}$, cell body velocity v_c, retrograde flow velocities $v_{rf}, v_{r,b}$, and protrusion edge forces $F_{f,b}$ are determined by algebraic equations of $L_{f,b}$ and $\kappa_{f,b}$, all listed in the supporting material. Algebraic equations also relate the parameters of these dynamics to integrin signaling and the FN density.

Motivated by the observations presented in Fig. 1, we formulate a cell model with front and back protrusions moving on a 1D FN lane (Fig. 2 *A*). The model is based in part on our previous work on steady cell motion by Schreiber et al. (35). The main extensions of the model compared with Schreiber et al. (35) are the cell body, the back protrusion, and the noisy clutch. The requirement for the noisy clutch from a modeling point of view follows from the dynamics we consider here, while we considered stationary properties in (35).

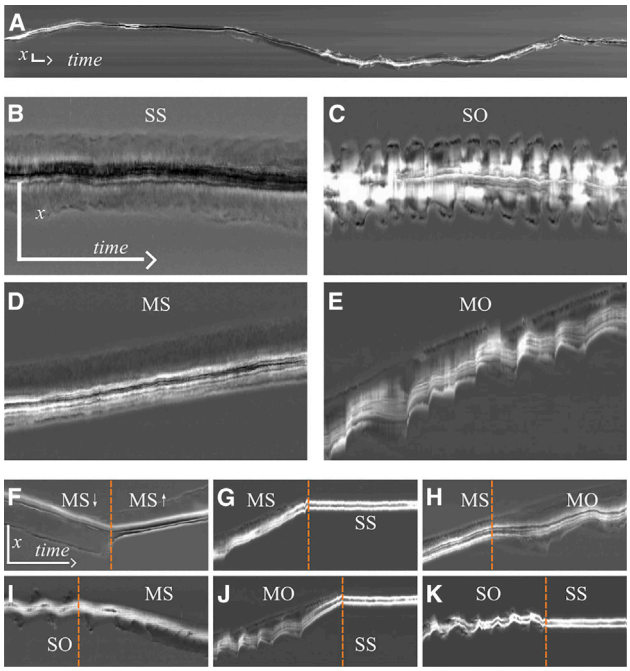

FIGURE 1 Four dynamic states and two motion directions form the multistability of MDA-MB-231 cells on homogeneous fibronectin lanes. (*A*) Kymograph from a typical 48-h trajectory. (*B*) A spread (S) cell with steady length (S). We call this state SS. (*C*) A spread cell with oscillatory length (O). We call this state SO. (*D*) A moving cell (M) with steady length: state MS. (*E*) A moving cell with oscillating length: state MO. (*F*) Transition from a downward-moving MS state to an upward-moving MS state. (*G–K*) The cells undergo an MS → SS (*G*), MS → MO (*H*), SO → MS (*I*), MO → SS (*J*), and SO → SS (*K*) transition. Vertical orange lines indicate the point in time of the state transitions as determined by the change point algorithm described in section S2. All kymographs are shown with a time resolution of 30 s. Time goes from left to right. The vertical scale bars represent 100 μm, the horizontal scale bars 60 min. The scale bars in (*B*) apply to (*B–E*), and the scale bars in (*F*) apply to (*F–K*). The movies corresponding to kymographs (*A–F*) can be found in the supporting material. To see this figure in color, go online.

The force balances (see Eqs. S2–S4 and Fig. 2 *A*) applied to the front and back edges and cell body have been established in a variety of studies (20–22,63,66–69). They comprise the drag forces resisting motion $\zeta_{f,b}v_{f,b}$ and $\zeta_c v_c$, the retrograde flow friction force $\kappa_{f,b}v_{r,f,b}$, and the elastic forces (Fig. 2 *A*). The drag coefficients $\zeta_{f,b,c}$ and the retrograde flow friction coefficients $\kappa_{f,b}$ are affected by adhesion and integrin signaling (Eqs. 2, 3, S17, and S18). The cell body velocity v_c is determined by the forces acting on it from front and back protrusions and the drag coefficient of the cell body ζ_c.

We choose a linear dependency of the force between protrusion edges and cell body on the protrusion length (elastic force) based on the results in (35) (see Eqs. S2–S4 and (51)). We assume that the force is transmitted by membrane tension and consider as its most likely cause volume homeostasis in 1D (70).

The network extension rate v_e is equal to the vectorial difference of the edge velocity and retrograde flow velocity. It is fixed by polymerization, which is force dependent with the well-known Arrhenius factor (66,68,71) (see Eqs. S5 and S6).

The lengths of the protrusions $L_{f,b}$ are dynamic due to velocity differences between the edges and the cell body:

$$\frac{dL_f}{dt} = v_f - v_c, \frac{dL_b}{dt} = v_c - v_b. \tag{1}$$

The noisy clutch has been reported in a variety of studies (64,72–79) and is due to the retrograde motion of the treadmilling F-actin network inside the protrusion (17,80,81). This flow causes friction with all structures relative to which it moves, in particular also with stress fibers and the intracellular interface of adhesion sites (75,82,83). The friction of the F-actin flow transmits the protrusion force to the substrate (22,32,75,77,82–85). The value of the friction coefficient can be perceived as the state of the clutch, with large values corresponding to an engaged state and low values to a disengaged state.

The relation between friction force and retrograde flow velocity exhibits increasing friction force at small velocities up to a critical velocity value $v_{r,cr}$, beyond which friction force decreases (Fig. 2 *A* and Eq. S19). The force maximum entails stick-slip transitions of sudden acceleration at the critical velocity due to the decrease of the force-resisting motion while the force-driving motion is maintained. Stick-slip behavior is a versatile phenomenon generating sound in bowed string instruments (86,87), causing earthquakes (88), and leading to wear in articular joints (89). Recent theoretical studies suggested it to be relevant also for protrusion dynamics (51,61,62,64,90,91) and polarization (51,62,90). Chan and Odde (92) and Wolgemuth (93) investigated the role of myosin-generated force and substrate stiffness in the clutch dynamics.

The friction force is proportional to the number of transient bonds between the F-actin network and stationary structures in the protrusion. Its biphasic character is due to fast dissociation of these bonds at fast retrograde flow (the clutch disengages) (94). They have to rebind to reach their equilibrium density after a high-velocity phase. This motivates the κ dynamics adapted from (64)

$$\frac{d\kappa_f}{dt} = c_1\left(\kappa_f^{\lim} - \left(\kappa_f - \kappa_0\right)\right) - c_2 e^{\frac{|v_{r,f}|}{c_3}}\left(\kappa_f - \kappa_0\right) + \eta_f(t), \tag{2}$$

$$\frac{d\kappa_b}{dt} = c_1\left(\kappa_b^{\lim} - \left(\kappa_b - \kappa_0\right)\right) - c_2 e^{\frac{|v_{r,b}|}{c_3}}\left(\kappa_b - \kappa_0\right) + \eta_b(t), \tag{3}$$

with an exponential acceleration of bond dissociation by retrograde flow velocity $c_2 e^{\frac{|v_{r,b}|}{c_3}}$ (94).

The maximum values $\kappa_{f,b}^{\lim}$ of $\kappa_{f,b}$ and $\zeta_{f,b}$ exhibit a Hill-type relation to the FN substrate density $B_{f,b,c}$, as specified by Eqs. S17 and S18. This

type of relation has been concluded from an earlier analysis of the adhesion-velocity relation (35). As justified in detail in the section "transitions between cell states," we assume that bond formation and breakage cause some noise on top of the deterministic dynamics, and add the noise terms $\eta_f(t)$ and $\eta_b(t)$ (see also Eq. S16). The stationary states of Eqs. 2 and 3 represent the biphasic friction force-retrograde flow velocity relation Eq. S19. The detailed equations are provided in the supporting material. The parameter values of the model are listed in Table S2.

RESULTS

Dynamic cell states

We monitored MDA-MB-231 cells migrating in FN-coated lanes over 48 h using scanning time-lapse microscopy. As described in materials and methods, rows of fields of view are sequentially imaged with 10-min or 30-s intervals per round collecting data from 144 to 16 fields of view, respectively, with on average 23 single-cell trajectories per field of view. The average single-cell trajectory length is 11.6 $\pm$ 8.0 h, limited by the fact that cells divide. We analyze in total more than 20,000 trajectories (10 min resolution) and 6000 cell trajectories (30 s resolution) (see Table S1 and Fig. S1. A representative 48-h kymograph of the 1D cell motion is depicted in Fig. 1 *A* (see also Video S1).

As described in more detail below, we observe four distinct dynamic states (Fig. 1, *B–E* and Videos S2, S3, S4, S5, and S6): a spread state with steady length (SS), a spread state with oscillatory protrusions at both ends (SO), a moving state with steady length (MS), and a moving state with an oscillating back protrusion (MO). The two moving states exist as moving up and down, so that we observe six states in total. We also exemplify six different state transitions, all of which occur on homogeneous FN lanes and without any stimulation. Therefore, we call them spontaneous transitions. The states SS and MO have also been found with RPE1 cells and NIH-3T3 fibroblasts (51), and all four dynamic states with C6 glioma cells. The oscillatory dynamics in SO and MO do not exhibit a regular period in many cases. This irregularity of repetitive protrusion events indicates a noisy excitable regime rather than regular oscillations in the strict sense of dynamical systems theory. We will see in the following section that we find regular oscillations, noisy oscillations, and a noisy excitable regime in our biophysical model.

Spread cells are symmetric and exhibit protrusions at both ends. Moving cells of course display protrusions at the front. However, we can identify additional back protrusions easily by the occurrence of negative back edge velocities in the oscillatory states, as shown by the cells in Fig. 1, *E* and *J*. Hence, moving oscillatory cells also exhibit protrusions at the front and back. We cannot tell from Fig. 1 *F* whether a protrusion exists at the back of a cell in state MS while it moves steadily. If steady protrusions at the back exist, they are most likely shorter than front protrusions (see below). However, the emergence or extension of a back protrusion precedes the direction reversal in Fig. 1 *F* by about 30 min. Hence, protrusions at front and back exist at the time of the transition, which supports the idea of direction reversals being the result of the competition of front and back protrusions, as we will see below.

Analysis of dynamic cell states

We analyze cell states on the basis of our biophysical model. Its components are explained in Fig. 2, and the equations are introduced in materials and methods and the supporting material. Eqs. 1, 2, and 3 together describe the cell dynamics in terms of cell length and the retrograde flow friction coefficient κ determined by the number of bonds between the F-actin network and structures stationary in the lab frame of reference, i.e., the clutch state.

Our model reproduces the adhesion-velocity relation in agreement with experiments (Fig. 2 *B* and section S5). This relation has been discussed in detail in Schreiber et al. (35) for cells with one protrusion in the direction of motion. The reproduction of this fundamental relation by the two-protrusion model supports our choice of modeling of the effect of FN signaling on friction and drag forces. Our model with the parameter values of Table S2 exhibits only spread states at very small FN density. The experiments show spread and moving cells in this parameter range. We use strictly symmetric protrusions with regard to parameter values in our model. Our results in Schreiber et al. (35) show excellent agreement between an asymmetric model and experimental data also at small FN densities. On that basis, we assume that protrusion asymmetry in cells causes the difference between experiments and the symmetric model at low FN density. The model predicts a stationary force-velocity relation of cell motion as shown in Fig. 2 *C*. Our results are very similar to relations predicted earlier (35,63). All predictions agree on the point that this relation reflects the retrograde flow friction law (35,63).

Analysis of cell states starts with appointing stretches of trajectories to one of the four dynamic states. The method of state classification is explained in detail in section S2.1 and Fig. S2. It analyzes cell behavior described by kymographs. Deducing states from behavior requires definition of a minimal time of consistency. If the behavior qualifies for this time as belonging to a specific state, we appoint this state to the cell. We have chosen 1 h as this time (see section S2.1). We do not classify the state of simulated cells on the basis of the known dynamic regime of the model, but rather apply the same procedure to experimental and simulated data in order to maximize compatibility of outcome.

We draw our mechanistic conclusions on the basis of the agreement between model results and experiments. The model reproduces all four dynamic states of MDA-MB-231 cells (Fig. 3 *A*). Both quantitative characteristics with regard to fraction of cells in the different states (Fig. 3 *B*) such as oscillation period, oscillation amplitude, and

velocity, and qualitative ones such as the back edge but not the front oscillating in the moving state, are met by the model (Fig. 3, *A*, *E*, and *F*).

The force-generation machinery at front and back protrusions work asymmetrically in the motile states MS and MO. This polarization between protrusions does not require any signaling to be established. It is based completely on the mechanical properties of retrograde flow. Retrograde flow is always faster at the back than at the front, since it needs to keep up with cell motion (Figs. 2 *A* and S10). Therefore, the biphasic friction force-retrograde flow velocity relation (Fig. 2 and Eq. S19) entails that the strongest coupling between F-actin network and substrate via adhesion structures forms in the front protrusion. The value of κ_f is always higher and forces are stronger in the front protrusion than in the back protrusion (Fig. 3 *E*).

Driven stick-slip systems robustly generate oscillations (86,87). A stick-slip transition of the clutch is also here the core of the oscillation mechanism of the protrusions, similar to earlier studies (51,61,62). We describe this in detail in section S4 and also explain the role of parameters. Whenever the forces driving retrograde flow drive it up to v_{cr}, the flow slips, causing the peaks in edge velocity and retrograde flow rate in Fig. 3 *E* and *F* and a sudden drop of the friction coefficient and all forces. The recovery of κ thereafter is slow and takes the larger part of the period.

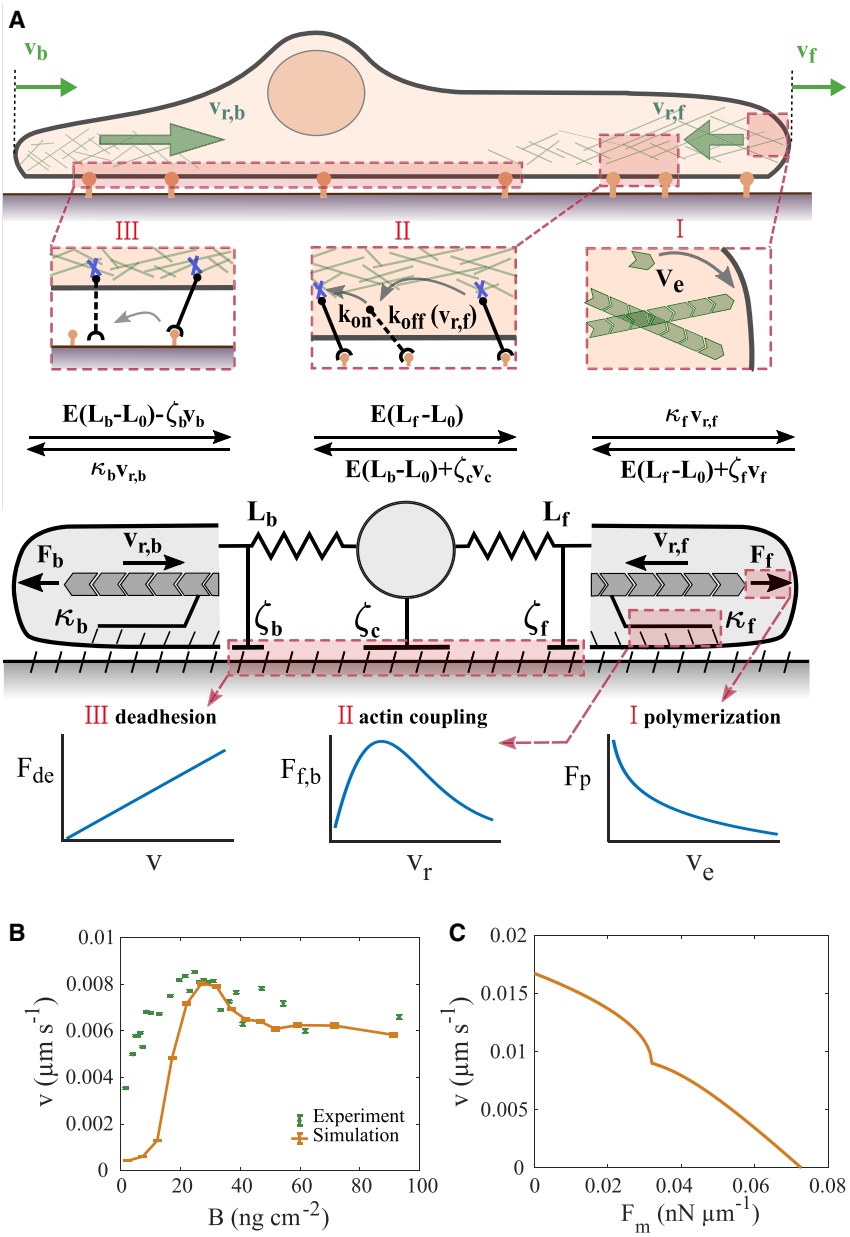

FIGURE 2 (*A*) Model constituents. Cartoon of a cell moving on a 1D fibronectin lane (*top*), force balances (*middle*), and the mechanical components of the model (*bottom*). Front and back protrusion edges move with velocities v_f and v_b, respectively. The F-actin networks flow with the retrograde flow rates $v_{r,f}$ and $v_{r,b}$, respectively. The forces $F_b = \kappa_b v_{r,b}$ and $F_f = \kappa_f v_{r,f}$ arise from polymerization of F-actin, act on the protrusion edge membrane, and drive retrograde flow against the friction forces. The front and back edge membrane experience drag with the coefficients ζ_f and ζ_b, respectively. Elastic forces $E(L_f - L_0)$ and $E(L_b - L_0)$ act between the cell body and the edges (equilibrium length L_0). The balance of the elastic forces determines the motion of the cell body against the drag force $\zeta_c v_c$. Bottom panels illustrate types of essential relations of the model. The de-attachment force of the back F_{de} is linearly related to velocity. The friction force between F-actin network retrograde flow v_r and stationary structures exhibits a maximum in its dependency on retrograde flow (clutch). The polymerization force F_p is logarithmically related to the network extension rate v_e due to the force dependency of the polymerization rate. (*B* and *C*) Two constitutive relations. (*B*) The adhesion-velocity relation. Green dots represent experimental data (see Table S1 and Data S7). Error bars represent the standard error of the mean. (*C*) The stationary force-velocity relation predicted by the model for $B = 45$ ng cm^{-2} (see section S10 for details). It provides the cell velocity under constant application of the external force F_m to the leading edge or cell body. Parameter set 1 from Table S2 is used for both panels. To see this figure in color, go online.

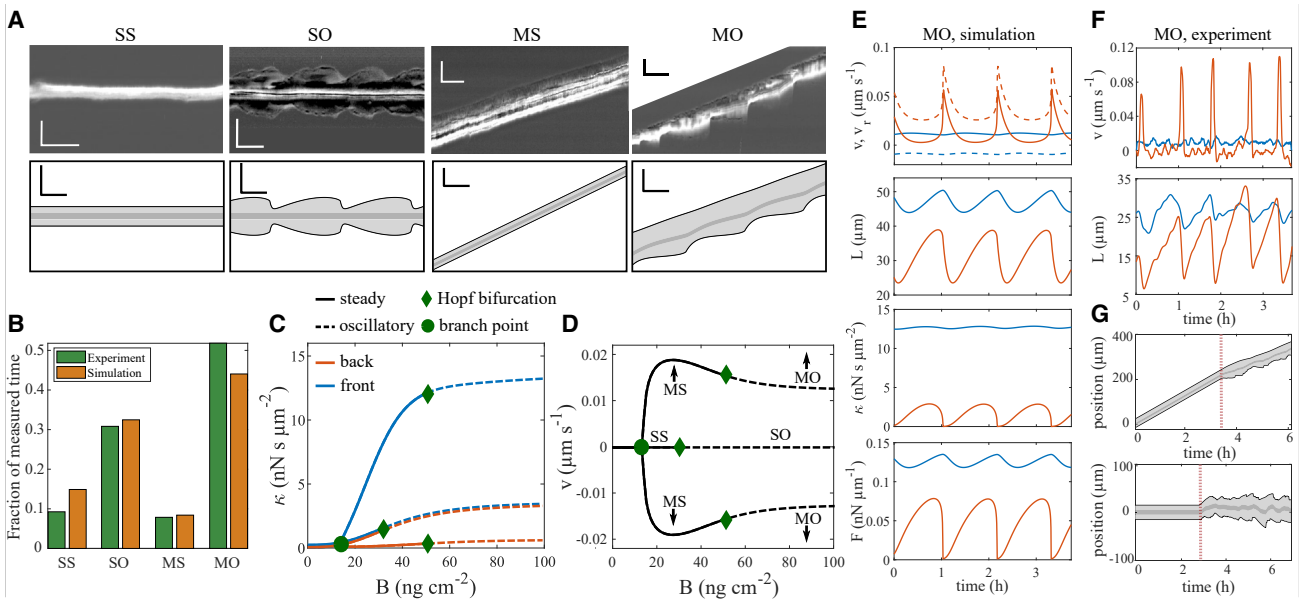

FIGURE 3 Analysis of dynamic cell states. They are either spread (SS, SO) or moving (MS, MO), and either steady (SS, MS) or oscillatory (SO, MO). (*A*) Upper panels show experiments, lower panels simulations without noise. Horizontal scale bars represent 30 min, vertical scale bars 50 μm. The cut corner of the experimental MO state showed another cell. Simulations used $c_3 = 0.0088\ \mu\text{m s}^{-1}$, SS, MS $B = 22$ ng cm^{-2}, SO $B = 36$ ng cm^{-2}, MO $B = 80$ ng cm^{-2}. (*B*) Fraction of cells in the cell states in experiment (2878 h of trajectories) and in simulations sampled from experiments on a range of fibronectin concentrations (see section S1.2 for details). (*C* and *D*) Cell states of the noise-free model illustrated by their value of the friction coefficient κ in the stationary state (*C*) and the cell velocity v (*D*) for fibronectin concentration B. Only the state SS exists at low B. At the concentration denoted as branch point, moving states appear and coexist with the spread state. Oscillations start (*dashed lines*) at the fibronectin concentrations marked as Hopf bifurcations. All moving states exist as moving up and down (*D*). (*E*) Simulation without noise of the time course of edge velocity v (*solid line*), retrograde flow v_r (*dashed line*), cell length L, friction coefficient κ, and force on the edge membrane F in state MO (*blue front*, *orange back*). (*F*) Measured time course of edge velocity and cell length in state MO (*blue front*, *orange back*). (*G*) The steady states MS (*upper panel*) and SS (*lower panel*) are excitable. They behave steadily with noise-free dynamics. Noise is switched on at the time marked by the red line. It causes behavior very similar to noisy oscillations (Fig. S5). Parameters of all simulations are listed in set 1 in Table S2.

Retrograde flow velocity v_r is equal to the network extension rate in the state SS. It is a tense state with two balanced opposing forces. This tense state is unstable against supercritical fluctuations in κ, which may arise from the concurrent snapping or formation of bonds between the F-actin network and stationary structures, and other perturbations as we will see below. The protrusion goes through one protrusion-retraction cycle upon a sufficiently strong perturbation. If these perturbations occur randomly, they are called noise. Chemical noise from random formation and breakage of bonds is omnipresent and represents relevant perturbations in systems as small as protrusions (95). The relevance of noise for adhesion and retrograde flow dynamics has been demonstrated by a variety of studies (64,90,91,96,97).

States in which small (but supercritical) perturbations may cause a large response are called excitable. Both the states SS and MS are excitable (Fig. 3 *G*). The protrusion-retraction cycle after a perturbation in the excitable regime is very similar to the oscillation cycle of noisy oscillations (Fig. S5). Therefore, the permanent noise in the bonds between the F-actin network and adhesion structures may cause oscillation-like behavior in the model cells even if they are in states SS and MS (Fig. 3 *G*). Whether the noise is supercritical—causing oscillations—or not depends on the specific parameters of the cell and the noise amplitude. Thus, the states SS and MS with low noise amplitude coexist with oscillation-like states at higher noise amplitude.

The experimental and simulated oscillations shown in Fig. 3 *A* are both rather smooth with subcritical noise, but noise may have a strong effect on state MO as we show in Fig. S5. It not only renders the time course irregular but also substantially shortens the average period. Interestingly, we find examples for both smooth (Fig. 3 *A*) and noisy oscillations (Fig. 1) in the experimental data indicating that noise amplitude is a cellular parameter and varies between individual cells. Accordingly, we have put the model noise in the clutch mechanism of retrograde flow, which is an intracellular process.

Fig. 3 *C* shows the existence of the dynamic states of the noise-free model cell in a systematic way for a range of FN coating densities. At coating densities below the value of B marked as branch point, only the spread state SS exists. Above it, spread and moving states coexist. Coexistence of several observable states for one set of parameters is multistability. At the FN density values marked as Hopf bifurcation points, oscillations start and we observe the states SO and MO. Between the branch point and the Hopf bifurcation of the spread branch, the spread state SS and moving state MS

coexist. The Hopf bifurcation of the spread state occurs at smaller FN density (B) than the one of the moving state, and thus we find a range of coexistence of SO and MS. This order of bifurcation points is swapped at other parameter values and, therefore, SS can also coexist with MO (see Fig. S5 and section S6). SO and MO coexist at large B values.

An individual cell is described in the model by a set of parameter values. The population of cells in a given experiment represents many different parameter value sets due to cell-to-cell variability. Therefore, we may find all possible pairings of coexistence in a single experiment, and both moving states can coexist with both spread states (Figs. 3 *C* and S5).

In correspondence to its versatile experimental observation, multistability of the four morphodynamic states appears to be a very robust property of mathematical models of cells on 1D lanes including the clutch. Sens (62) and Ron et al. (61) also report very similar steady and oscillatory states (but not the excitable regime) and their coexistence in noise-free models. Hennig et al. report the states SS and MO and the irregularity of oscillations in a noisy stick-slip model (51).

Transitions between cell states

All possible transitions are illustrated in Fig. 4 *A*. The fractions of transitions out of a given state are shown in Fig. 4 *B* for the experimental data. The simulations in Fig. 4 *C* show good agreement with the measurements. The same applies to the comparison of theory and experiment with latrunculin A and blebbistatin applied, shown in Fig. S7.

Transitions between the dynamic states demonstrate that an individual cell can be in different states at given fixed conditions (or at the same parameter values in modeling terms). They are the experimental manifestation of multistability. The multistability in the biophysical model is shown in Figs. 3, *C* and *D* and S5. Both spread states SS and SO can coexist with either MS or MO in the biophysical model. The upward-moving states coexist with their downward-moving analogs (Fig. 3 *C*).

Transitions between these coexisting cell states are caused by noise in the adhesion variable in the biophysical model. For several reasons we assume that noise causes also the transitions in the MDA-MB-231 cells. Cells with their typical volume in the femtoliter range are microscopic systems subject to thermal noise in many aspects of their behavior (98–101). Since adhesion sites are discrete spots, their length scales are even two orders of magnitude smaller than cell size, rendering them even more susceptible to thermal noise. Our model results show that we can reach good agreement between theory and experiment by noise in the clutch mechanism of retrograde flow. In addition, transitions occur apparently spontaneously on homogeneous FN lanes without any obvious signaling event or stimulation.

We showed above that both motile states can coexist with both spread states in the model. However, SS does not coexist with SO, and neither does MS coexist with MO in

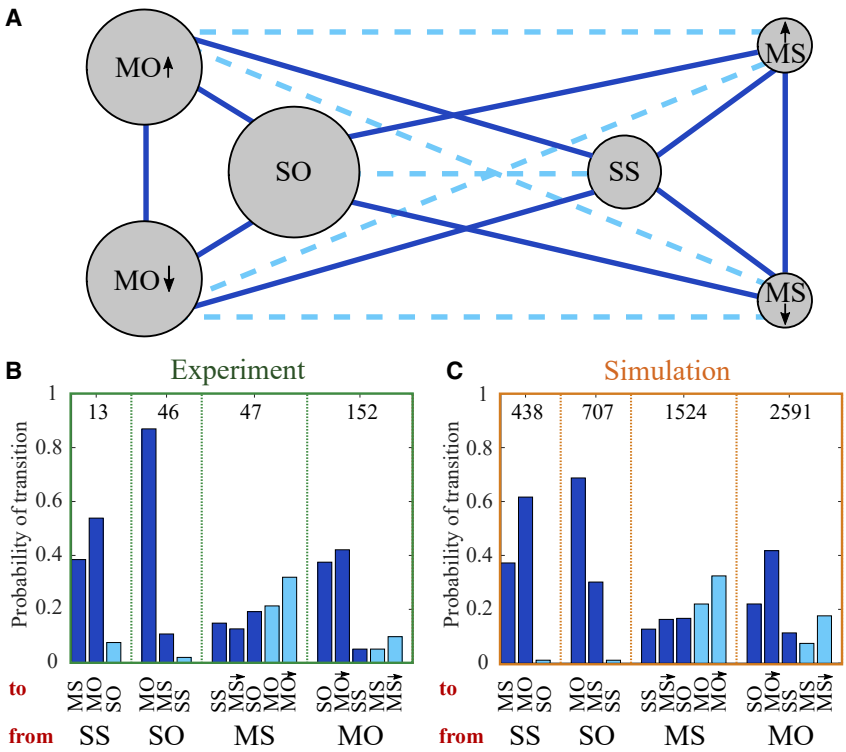

FIGURE 4 The transitions between the cell states. (*A*) The states MS moving steadily, MO moving oscillatory, SS spread steadily, and SO spread oscillatory are introduced in Fig. 3 and the text. Arrows distinguish moving up and down. The areas of circles are proportional to the fraction of cell states in experiments. Solid lines mark transitions in the sense of dynamical systems theory of multistability, i.e., between states coexisting in the noise-free mathematical model taking cell variability of parameter values of ±5% about the reference parameter set into account (see Fig. S5, section S6, and section S1.2). The state changes along dashed lines are explained in the text. (*B* and *C*) Statistics of state transitions in experiments (*B*) and simulations (*C*). The bars belonging to a specific state listed at the bottom of the panel show the fraction of transitions out of this state to one of the other states. Transition types are color-coded as in (*A*). MO↓ and MS↓ indicate direction change in the transition. Analogous results with experimental data with blebbistatin and latrunculin A applied are provided in Fig. S7. Sample size is indicated by the numbers inside the chart. Parameters of all simulations are listed in set 1 of Table S2. To see this figure in color, go online.

the bifurcation schemes in Figs. 3 *C* and S5. How, therefore, do we see transitions within these pairs of states in experimental and simulated data?

Oscillation-like protrusion events in the excitable regime occur randomly. Because of this randomness, cells may exhibit the characteristics of steady behavior for a time sufficiently long to qualify as a state and then switch to oscillation-like behavior, or vice versa. Thus, steady ↔ oscillatory transitions come out of the state analysis of the data. However, they are not state transitions in the sense of dynamical systems theory for multistable systems. Simulated and measured data behave very similar in regard to state classification and transitions, including steady ↔ oscillatory transitions. Therefore, the mechanistic ideas formulated in the model reproduce the statistics of state transitions both in the sense of multistability and the statistics of phases of consistent behavior of MDA-MB-231 cells.

The identification of steady ↔ oscillatory transitions in simulated data implies that their occurrence in experimental data does not necessarily indicate parameter value changes. Changing parameter values might be an additional reason for these transitions in experiments, since cells constantly develop and their cellular parameter values might change within the duration of an experiment of up to 48 h.

This section dealt with spontaneous state transitions. We present state transitions caused by FN steps in section S11. The biophysical model also offers an explanation for their characteristics.

Reversal of direction and the UCSP

Fig. 5 *A* shows front and back edge velocity during a direction reversal averaged over many such events including both MS and MO reversals (see Fig. S10 for the retrograde flow and Fig. S4 *E* for the network extension rate). The moment of reversal t_{rev} is the time when the cell nucleus changes direction of motion. The back edge starts to slow down about 10 min prior to t_{rev} and is already moving in the new direction (negative velocity) at the time of reversal. The front slows down after the back edge. It still moves in the old direction at t_{rev} and reverses direction only a few minutes later. Finally, it collapses in an event appearing as a negative velocity peak in Fig. 5 *A*. After the recovery of the protrusion, both edges move in the new direction with the same velocity. In agreement with this scenario, the likelihood of back protrusions increases before t_{rev} and the frequency of occurrence of front collapses after t_{rev}. Both experiments and simulations show the same scenario. A supercritical protrusion event at the back pulls sufficiently strongly to collapse the front protrusion. The back protrusion event is caused by noise in the MS state. In the MO state, protrusions occur periodically but noise generates supercritical protrusion events. We discuss forces and retrograde flow during reversal events additionally in section S9 and Figs. S5, S10, and S11.

Random direction reversals in 1D and direction changes in 2D or 3D are one reason why cells do not move permanently in their initial direction. Hence, the statistics of direction reversals and changes shape the UCSP, which we show in Fig. 5 *B* for the MDA-MB-231 cells in 1D. We find an increase of persistence time with cell velocity (in agreement with earlier results (36)). Application of latrunculin A increases persistence time. Latrunculin reduces the F-actin polymerization rate, and its application has been modeled accordingly by decreasing the force free polymerization rate V_e^0 (set 2 in Table S2). We find good agreement between experiment and simulations both for control and latrunculin A conditions, and also with blebbistatin applied (see Fig. S8).

The velocity scenario in Fig. 5 *A*, the observation that direction reversals happen only when protrusions at the front and back exist, and a strong robustness of the front protrusion against noise at the front all suggest direction reversal events to arise from competition between the front and back protrusions. As a first step in disentangling the competition mechanism, we provide a picture of protrusion stability exemplified by the state MS. The values of the two dynamic variables friction coefficient κ and protrusion length L describe the state of the model protrusions. Upon a perturbation away from its steady state, a protrusion might just go back to the steady state or collapse (Figs. 5 *C* and S9). The basin of attraction in a κ-L plot quantifies these two possibilities. If the protrusion is perturbed to a state within the basin of attraction, it relaxes back to the steady protrusion state. It collapses upon larger perturbations. Fig. 5 *C* shows that the basin of attraction of the front protrusion of fast cells is larger than the one of slow cells and vice versa for the back protrusion. Hence, the front protrusion is more stable in fast cells than in slow ones, and the back protrusion is less stable in fast cells than in slow ones.

The pulling of the back protrusion on the nucleus and the front protrusion during the direction reversal scenario described above increases the elastic force acting on the front edge membrane. This force increase speeds up retrograde flow. If the back pulls strongly enough, it drives retrograde flow velocity to the decreasing branch of the friction force-v_r relation (see Fig. 2) and shifts the state of the front protrusion from the stationary state to a trajectory outside the basin of attraction, which entails the collapse. The collapse is a rapid decrease of κ due to breaking of bonds between the F-actin network and stationary structures followed by rapid shrinkage of protrusion length due to the elastic force as shown in Fig. 5 *C* (see also the description in section S8). Remarkably, the stochastic event inside the back protrusion, which in the end causes the front protrusion collapse and direction reversal, typically occurs minutes before the moment of direction reversal.

The back pulls on the front by protruding (Fig. 5 *A*), i.e., by going through an excitation in the MS state. The slower the retrograde flow in a back protrusion, the longer the

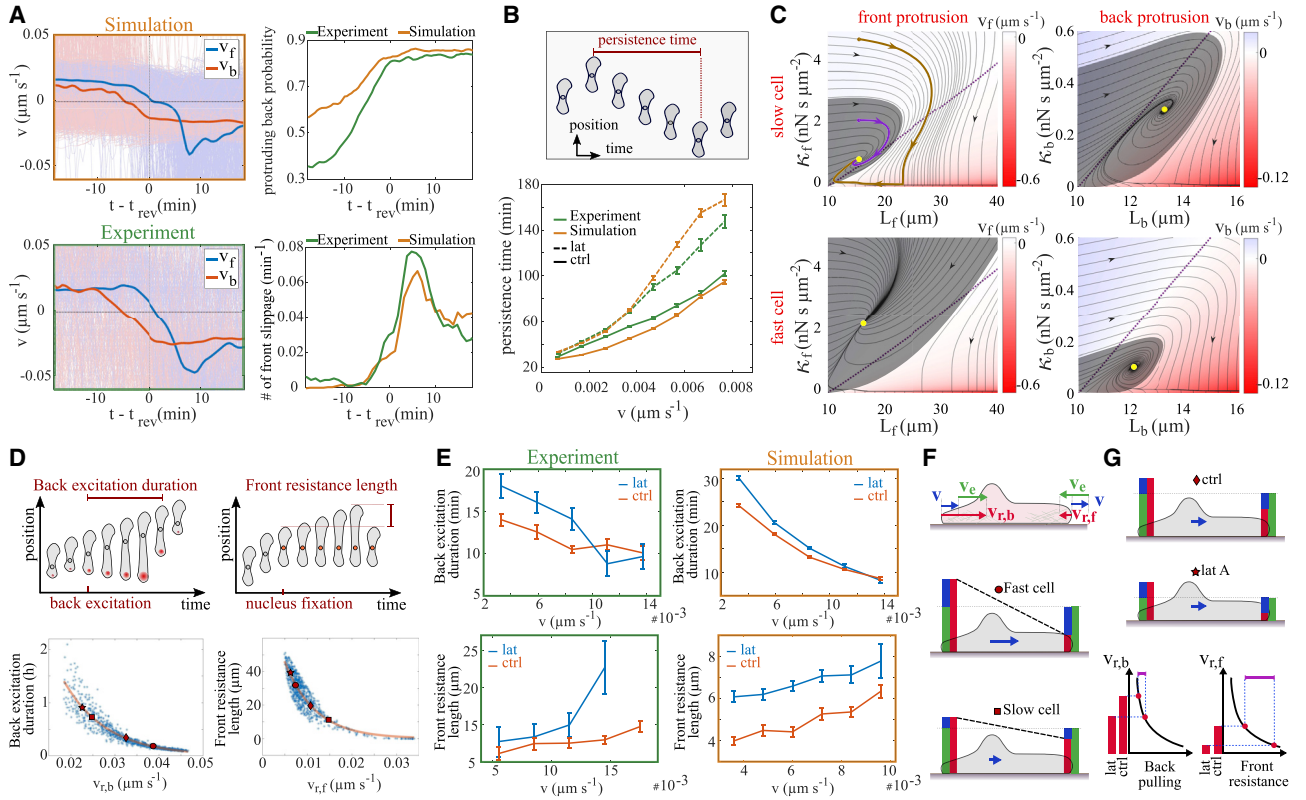

FIGURE 5 Direction reversal mechanism. (*A*) Front (v_f) and back (v_b) velocities during reversal transitions averaged over many tracks (*thin lines*, 221 experimental trajectories), including both MS and MO states. The cell nucleus changes direction at t_{rev}. For an illustrative example, see Fig. 1 *F* and the corresponding Video S6. (*B*) The relation between cell velocity and persistence time in control cells (9497 experimental trajectories) and with latrunculin A applied (3368 experimental trajectories). Latrunculin A application was modeled by decreasing the network extension rate V_e^0 from 0.030 to 0.022 μm s^{-1}. (*C*) Basin of attraction of the steady protrusion state (*gray area*) and state trajectories (*black lines*) in κ-L plots. Trajectories outside the basin of attraction (*brown*) go to small values of the friction coefficient κ and then to small protrusion length L with fast retrograde flow, which is the collapse. Trajectories starting within the basin of attraction (*purple*) lead to the steady state (*yellow dot*) without collapse. B is 20 ng cm^{-2}; velocities of fast and slow cells are 0.015 and 0.005 μm s^{-1}, respectively. (*D*) Cartoons illustrating definitions of duration of back excitation and front resistance length. Lower panels show simulations of these characteristics. Each dot marks the result of a simulation with parameter values randomly drawn from large parameter ranges (see section S1.2). (*E*) The relation between duration of back excitation and cell velocity, and front resistance length and cell velocity, in experiments and simulations (221 control experimental trajectories, 127 latrunculin A experiments). (*F*) Cartoon relations between velocities. Network extension rate (*green*) is the sum of cell velocity (*blue*) and retrograde flow velocity (*red*) in the front protrusion. Retrograde flow velocity is the sum of extension rate and cell velocity in the back protrusion, and therefore is always faster than retrograde flow in the front protrusion. (*G*) Cartoon illustrating the effect of latrunculin A. It reduces the network extension rate. Therefore, latrunculin A-treated cells have slower retrograde flow than control cells with the same cell velocity (colors as in *F*). This increases back pulling slightly and front resistance substantially (compare *D*) and thus renders the cells more persistent than control cells. Parameters of simulations in Table S2 (sets 1 and 2 for control and latrunculin conditions, respectively). Error bars represent standard error of the mean.

excitation lasts (Fig. 5 *D*). Whether it can collapse the front is determined by how long the front can resist the pulling. The slower the retrograde flow in the front protrusion, the longer it can resist. Symbols mark the retrograde flow values of typical fast and slow cells. Back excitations of fast cells are shorter, and their fronts can resist longer than slow cells. These properties of front and back protrusions hold for a large parameter range, i.e., these relations between stability characteristics and retrograde flow are fundamental and robust features.

The front resistance length is the length the front edge moves after motion arrest of the cell body. Fig. 5 *E* compares values for the duration of back excitation and front resistance length between our experimental data and simulations, and shows the qualitative agreement. Fig. 5 *F* summarizes our insights from the individual investigations. Fast cells have slow retrograde flow in the front protrusion and very fast retrograde flow in the back. This entails strong front protrusions and short excitations at the back and, hence, long persistence times. Slow cells have slower retrograde flow at the back and faster retrograde flow at the front, causing long back excitations and short front resistance length. They are therefore less persistent.

At a given velocity, latrunculin A increases persistence (Fig. 5 *B*). Application of latrunculin reduces the network extension rate and therefore reduces retrograde flow both at front and back compared with the control. This increases the duration of back excitations but even more the resistance

time and resistance length of the front, and thus renders the cell more persistent (see Fig. 5, *B* and *E* for experimental data and simulations). Fig. 5 *G* summarizes the latrunculin action graphically. We conclude that reducing network extension rate increases persistence, in agreement with our mechanistic ideas.

In summary, the protrusion competition mechanism based on elastic mechanical interaction between protrusions and cell body, nonlinear friction of retrograde flow (clutch), and noise in the clutch mechanism offers an explanation for the UCSP. The faster cells move, the slower is retrograde flow in the front protrusion, the faster is it in the back protrusion, and the more persistently the cell migrates.

DISCUSSION

We analyzed multistability of MDA-MB-231 cells on FN lanes and found in our experiments coexistence of states with oscillatory or steady cell shape, spread or moving, and moving up or down. We combined the experiments with quantitative theory, which suggests mechanistic ideas for several basic and general observations of mesenchymal motility comprising the biphasic adhesion-velocity relation, stationary force-velocity relation, UCSP, random migration, and steady, oscillatory, or excitable morphodynamics. Restricting cell motion to 1D made the relation between basic phenomena of cell motility very obvious. Random migration and the UCSP arise from random state transitions between the states "moving up" and "moving down," and the control of the parameters of the noisy clutch by integrin signaling generates the biphasic adhesion-velocity relation.

Our theory comprises three constituents, all of which are well-established experimental observations. The first one is the force balance at the protrusion edge (Eqs. S2–S4). It establishes the link between polymerization rate, cell velocity, and retrograde flow velocity (20–22,66–68). The second constituent is the noisy nonlinear friction between retrograde flow of the F-actin network and stationary structures (Eqs. S13 and S14) known as the clutch mechanism (64,75–79), which is crucial for oscillatory dynamics and multistability. Given a cell with protrusions at the front and back and symmetry with regard to parameters of the protrusions, the clutch mechanism introduces the mechanical polarization into a front protrusion with slow retrograde flow and a back protrusion with fast retrograde flow (62,90). We find that noise in the clutch mechanism due to random bonds between the F-actin network and stationary structures suffices to offer an explanation for state transitions and, thus, for the UCSP.

Multistability, oscillations, and mechanical polarization are all generated by the interaction of nonlinear F-actin flow dynamics and membrane tension without any signaling processes. Signaling sets the parameters of this system and thus determines the dynamic regime (steady, excitable, or oscillatory) and the cell velocity. A representation of the net effect of integrin signaling on drag and friction coefficients by Hill functions is the third constituent of the theory (Eqs. S17 and S18). Integrin signaling together with friction and force balance determine the adhesion-velocity relation (35). We know from Schreiber et al. (35) that a large part of cell-type-specific detail enters via this signaling constituent.

To support the idea that one mechanism explains the variety of observations, we followed the parameterization strategy to use one parameter set for all experiments with comparable conditions rather than fitting each experiment as well as possible. We were able to reach good quantitative agreement between simulations and experimental results with a single parameter set for control experiments and changes to parameter values describing drug applications corresponding to the known biochemical action of the drug. We were able to reach good agreement with regard to the types of states, the (temporal) characteristics of states, state fractions and transition probabilities, characteristics of reversal behavior, the UCSP, protrusion stability, the adhesion-velocity relation, and the behavior on FN steps. The large variety of observations agreeing between theory and experiment is a major reason for our assumption that we assembled the model constituents dominating the observed behavior, and that the mechanisms we suggest recapitulate the cellular processes. We review and discuss alternative mechanisms from literature in section S13.

Our experimental data confirm the UCSP for MDA-MB-231 cells and thus add another cell type to the many listed in Maiuri et al. (36) obeying this relation. Fast cells are more persistent than slow ones. Maiuri et al. explain the UCSP by a mechanism centered around the network extension rate: the fast network extension in fast cells advects an F-actin-binding inhibitor of network growth away from the protrusion tip and thus renders random protrusion collapse unlikely. Maiuri et al. conclude that the faster the network extension rate, the more persistently the cell moves (36). However, the data in Maiuri et al. from mature bone marrow dendritic cells migrating in a confined environment exhibiting a positive correlation between network extension rate and persistence time do not obey the UCSP (36). Furthermore, an endogenous F-actin-binding inhibitor of network extension has not been identified. Contrary to these ideas, reduction of the network extension rate by latrunculin entails an increase in persistence in our experiments and model. We found retrograde flow to be the most important indicator of stability (Fig. 5 *D*). With our approach and our data, the noisy clutch is sufficient to explain the UCSP by spontaneous direction reversals based on protrusion competition.

The mechanism suggested by Maiuri et al. implies that increasing network extension rate necessarily accompanies increasing protrusion velocity, i.e., the authors require proportionality of the velocities $v_e = av_f$ with a being constant across experimental conditions. Direct measurement of

protrusion velocity and retrograde flow in keratocytes (34) and PtK1 cells (26), and the theoretical analysis of adhesion-velocity relations for keratocytes, PtK1 cells, CHO cells, and MDA-MB-231 cells (35), come to the conclusion that this proportionality is violated. For example, increasing adhesion strength can reduce retrograde flow, entailing increasing protrusion velocity with constant or even decreasing network extension rate. Data by Jurado et al. (75) and Vicente-Manzanares et al. (12) report the relation $v_e = v_{r,f} + v_f$ (our Eq. S5), which is different from proportionality because all three velocities depend on experimental conditions (see also Fig. S4 *F*). Eq. S5 is obvious by geometrical reasoning (Fig. 2) and also compatible with a variety of measured adhesion-velocity relations (35).

The stationary force-velocity relation of cell motion represents the cell response to external force and, therefore, a basic cell property. Owing to technical problems of controlling either force or cell velocity to remain constant, it has not yet been measured, contrary to measurements and analyses of the dynamic relation, which allows both parameters to change during the experiment (20–22). Our results are very similar to relations predicted earlier (35,63). All predictions agree on the point that the stationary relation reflects the retrograde flow friction law (35,63).

CONCLUSION

We suggest as a main conclusion of our study that the basic phenomena of multistability with its dynamic regimes, adhesion-velocity relation, and UCSP can all be explained on the basis of the three model constituents force balance at the protrusion edges, noisy clutch, and integrin signaling. They also entail a specific prediction for the stationary force-velocity relation of cell motion. All three model constituents are observations which have been established earlier and in other contexts. Our study connects them and thus reveals their explanatory power. The universality of the model constituents offers a simple explanation for the universality of the constitutive relations.

DATA AVAILABILITY

Experimental data supporting the findings of this paper are available from the corresponding authors upon reasonable request. Source data of cell trajectories are provided as CSV files in the supporting material. A description of the data sets is available in section S1. Computational code is deposited on https://github.com/behnam89amiri/Multistability_and_constitutive_relations_of_cell_motion.

SUPPORTING MATERIAL

Supporting material can be found online at https://doi.org/10.1016/j.bpj.2023.02.001.

AUTHOR CONTRIBUTIONS

B.A. executed the theory and analyzed data; J.C.J.H. and C.S. executed experiments and analyzed data; M.F. designed and supervised theoretical research; J.O.R. designed and supervised experimental research; J.C.J.H., B.A., J.O.R., and M.F. wrote the paper. All authors have read and approved the published manuscript.

ACKNOWLEDGMENTS

We thank K. Rottner and T. Stradal, HZI Braunschweig, for stimulating discussions. This work was supported by the Deutsche Forschungsgemeinschaft (DFG201269156, SFB1032 to J.C.J.H., C.S., and J.O.R.).

DECLARATION OF INTERESTS

The authors declare no competing interests.

SUPPORTING CITATIONS

References (102–113) appear in the supporting material.

REFERENCES

1. Pollard, T. D., and G. G. Borisy. 2003. Cellular motility driven by assembly and disassembly of actin filaments. *Cell.* 112:453–465.
2. Abercrombie, M., J. E. Heaysman, and S. M. Pegrum. 1971. The locomotion of fibroblasts in culture: IV. Electron microscopy of the leading lamella. *Exp. Cell Res.* 67:359–367.
3. Ridley, A. J., M. A. Schwartz, …, A. R. Horwitz. 2003. Cell migration: integrating signals from front to back. *Science.* 302:1704–1709.
4. Insall, R. H., and L. M. Machesky. 2009. Actin dynamics at the leading edge: from simple machinery to complex networks. *Dev. Cell.* 17:310–322.
5. Lomakin, A. J., K. C. Lee, …, G. Danuser. 2015. Competition for actin between two distinct F-actin networks defines a bistable switch for cell polarization. *Nat. Cell Biol.* 17:1435–1445.
6. Dawes, A. T., and L. Edelstein-Keshet. 2007. Phosphoinositides and rho proteins spatially regulate actin polymerization to initiate and maintain directed movement in a one-dimensional model of a motile cell. *Biophys. J.* 92:744–768.
7. Yam, P. T., C. A. Wilson, …, J. A. Theriot. 2007. Actin–myosin network reorganization breaks symmetry at the cell rear to spontaneously initiate polarized cell motility. *J. Cell Biol.* 178:1207–1221.
8. Sheetz, M. P., D. P. Felsenfeld, and C. G. Galbraith. 1998. Cell migration: regulation of force on extracellular-matrix-integrin complexes. *Trends Cell Biol.* 8:51–54.
9. Lauffenburger, D. A., and A. F. Horwitz. 1996. Cell migration: a physically integrated molecular process. *Cell.* 84:359–369.
10. Huttenlocher, A., M. H. Ginsberg, and A. F. Horwitz. 1996. Modulation of cell migration by integrin-mediated cytoskeletal linkages and ligand-binding affinity. *J. Cell Biol.* 134:1551–1562.
11. Palecek, S. P., J. C. Loftus, …, A. F. Horwitz. 1997. Integrin-ligand binding properties govern cell migration speed through cell-substratum adhesiveness. *Nature.* 385:537–540.
12. Vicente-Manzanares, M., C. K. Choi, and A. R. Horwitz. 2009. Integrins in cell migration - the actin connection. *J. Cell Sci.* 122:199–206.
13. Parsons, J. T., A. R. Horwitz, and M. A. Schwartz. 2010. Cell adhesion: integrating cytoskeletal dynamics and cellular tension. *Nat. Rev. Mol. Cell Biol.* 11:633–643.
14. Burridge, K., and C. Guilluy. 2016. Focal adhesions, stress fibers and mechanical tension. *Exp. Cell Res.* 343:14–20.

15. Small, J. V., and J. E. Celis. 1978. Filament arrangements in negatively stained cultured cells: the organization of actin. *Cytobiologie.* 16:308–325.
16. Small, J. V., G. Isenberg, and J. E. Celis. 1978. Polarity of actin at the leading edge of cultured cells. *Nature.* 272:638–639.
17. Svitkina, T. M., A. B. Verkhovsky, …, G. G. Borisy. 1997. Analysis of the actin-myosin II system in fish epidermal keratocytes: mechanism of cell body translocation. *J. Cell Biol.* 139:397–415.
18. Small, J. V., T. Stradal, …, K. Rottner. 2002. The lamellipodium: where motility begins. *Trends Cell Biol.* 12:112–120.
19. Pollard, T. D. 2003. The cytoskeleton, cellular motility and the reductionist agenda. *Nature.* 422:741–745.
20. Prass, M., K. Jacobson, …, M. Radmacher. 2006. Direct measurement of the lamellipodial protrusive force in a migrating cell. *J. Cell Biol.* 174:767–772.
21. Heinemann, F., H. Doschke, and M. Radmacher. 2011. Keratocyte lamellipodial protrusion is characterized by a concave force-velocity relation. *Biophys. J.* 100:1420–1427.
22. Zimmermann, J., C. Brunner, …, M. Falcke. 2012. Actin filament elasticity and retrograde flow shape the force-velocity relation of motile cells. *Biophys. J.* 102:287–295.
23. Kage, F., M. Winterhoff, …, K. Rottner. 2017. FMNL formins boost lamellipodial force generation. *Nat. Commun.* 8:14832.
24. Keren, K., Z. Pincus, …, J. A. Theriot. 2008. Mechanism of shape determination in motile cells. *Nature.* 453:475–480.
25. Bretschneider, T., K. Anderson, …, G. Gerisch. 2009. The three-dimensional dynamics of actin waves, a model of cytoskeletal self-organization. *Biophys. J.* 96:2888–2900.
26. Barnhart, E. L., K.-C. Lee, …, J. A. Theriot. 2011. An adhesion-dependent switch between mechanisms that determine motile cell shape. *PLoS Biol.* 9:e1001059.
27. Schaub, S., S. Bohnet, V. M. Laurent, J.-J. Meister, and A. B. Verkhovsky. 2007. Comparative maps of motion and assembly of filamentous actin and myosin II in migrating cells. *Mol. Biol. Cell.* 18:3723–3732.
28. Shao, D., H. Levine, and W.-J. Rappel. 2012. Coupling actin flow, adhesion, and morphology in a computational cell motility model. *Proc. Natl. Acad. Sci. USA.* 109:6851–6856.
29. Ziebert, F., and I. S. Aranson. 2013. Effects of adhesion dynamics and substrate compliance on the shape and motility of crawling cells. *PLoS One.* 8:e64511.
30. DiMilla, P. A., K. Barbee, and D. A. Lauffenburger. 1991. Mathematical model for the effects of adhesion and mechanics on cell migration speed. *Biophys. J.* 60:15–37.
31. DiMilla, P. A., J. A. Stone, …, D. A. Lauffenburger. 1993. Maximal migration of human smooth muscle cells on fibronectin and type IV collagen occurs at an intermediate attachment strength. *J. Cell Biol.* 122:729–737.
32. Munevar, S., Y. Wang, and M. Dembo. 2001. Traction force microscopy of migrating normal and H-ras transformed 3T3 fibroblasts. *Biophys. J.* 80:1744–1757.
33. Mueller, J., G. Szep, …, M. Sixt. 2017. Load adaptation of lamellipodial actin networks. *Cell.* 171:188–200.e16.
34. Gupton, S. L., and C. M. Waterman-Storer. 2006. Spatiotemporal feedback between actomyosin and focal-adhesion systems optimizes rapid cell migration. *Cell.* 125:1361–1374.
35. Schreiber, C., B. Amiri, …, M. Falcke. 2021. On the adhesion–velocity relation and length adaptation of motile cells on stepped fibronectin lanes. *Proc. Nat. Acad. Sci. USA.* 118:e2009959118.
36. Maiuri, P., J.-F. Rupprecht, …, R. Voituriez. 2015. Actin flows mediate a universal coupling between cell speed and cell persistence. *Cell.* 161:374–386.
37. Giannone, G., B. J. Dubin-Thaler, …, M. P. Sheetz. 2004. Periodic lamellipodial contractions correlate with rearward actin waves. *Cell.* 116:431–443.
38. Döbereiner, H. G., B. J. Dubin-Thaler, …, M. P. Sheetz. 2006. Lateral membrane waves constitute a universal dynamic pattern of motile cells. *Phys. Rev. Lett.* 97:038102.
39. Gholami, A., M. Falcke, and E. Frey. 2008. Velocity oscillations in actin-based motility. *New J. Phys.* 10:033022.
40. Enculescu, M., A. Gholami, and M. Falcke. 2008. Dynamic regimes and bifurcations in a model of actin-based motility. *Phys. Rev. E - Stat. Nonlinear Soft Matter Phys.* 78:031915.
41. Enculescu, M., M. Sabouri-Ghomi, …, M. Falcke. 2010. Modeling of protrusion phenotypes driven by the actin-membrane interaction. *Biophys. J.* 98:1571–1581.
42. Allard, J., and A. Mogilner. 2013. Traveling waves in actin dynamics and cell motility. *Curr. Opin. Cell Biol.* 25:107–115.
43. Koestler, S. A., S. Auinger, …, J. V. Small. 2008. Differentially oriented populations of actin filaments generated in lamellipodia collaborate in pushing and pausing at the cell front. *Nat. Cell Biol.* 10:306–313.
44. Burnette, D. T., S. Manley, …, J. Lippincott-Schwartz. 2011. A role for actin arcs in the leading-edge advance of migrating cells. *Nat. Cell Biol.* 13:371–381.
45. Zimmermann, J., and M. Falcke. 2014. formation of transient lamellipodia. *PLoS One.* 9:e87638.
46. Barnhart, E. L., J. Allard, …, A. Mogilner. 2017. Adhesion-dependent wave generation in crawling cells. *Curr. Biol.* 27:27–38.
47. Bolado-Carrancio, A., O. S. Rukhlenko, …, B. N. Kholodenko. 2020. Periodic propagating waves coordinate RhoGTPase network dynamics at the leading and trailing edges during cell migration. *Elife.* 9:e58165.
48. Doubrovinski, K., and K. Kruse. 2011. Cell motility resulting from spontaneous polymerization waves. *Phys. Rev. Lett.* 107:258103.
49. Beta, C., and K. Kruse. 2017. Intracellular oscillations and waves. *Annu. Rev. Condens. Matter Phys.* 8:239–264.
50. Gerhardt, M., M. Ecke, …, G. Gerisch. 2014. Actin and PIP3 waves in giant cells reveal the inherent length scale of an excited state. *J. Cell Sci.* 127:4507–4517.
51. Hennig, K., I. Wang, …, M. Balland. 2020. Stick-slip dynamics of cell adhesion triggers spontaneous symmetry breaking and directional migration of mesenchymal cells on one-dimensional lines. *Science Advances.* 6:eaau5670.
52. Park, J., W. R. Holmes, …, A. Levchenko. 2017. Mechanochemical feedback underlies coexistence of qualitatively distinct cell polarity patterns within diverse cell populations. *Proc. Natl. Acad. Sci. USA.* 114:E5750–E5759.
53. Lee, S. H., J. C. Hou, …, A. Levchenko. 2022. A molecular clock controls periodically driven cell migration in confined spaces. *Cell Syst.* 13:514–529.e10.
54. Verkhovsky, A. B., T. M. Svitkina, and G. G. Borisy. 1999. Self-polarization and directional motility of cytoplasm. *Curr. Biol.* 9:11–20.
55. Hawkins, R. J., R. Poincloux, …, R. Voituriez. 2011. Spontaneous contractility-mediated cortical flow generates cell migration in three-dimensional environments. *Biophys. J.* 101:1041–1045.
56. Ziebert, F., S. Swaminathan, and I. S. Aranson. 2012. Model for self-polarization and motility of keratocyte fragments. *J. R. Soc. Interface.* 9:1084–1092.
57. Tjhung, E., D. Marenduzzo, and M. E. Cates. 2012. Spontaneous symmetry breaking in active droplets provides a generic route to motility. *Proc. Natl. Acad. Sci. USA.* 109:12381–12386.
58. Ruprecht, V., S. Wieser, …, C. P. Heisenberg. 2015. Cortical contractility triggers a stochastic switch to fast amoeboid cell motility. *Cell.* 160:673–685.
59. Kozlov, M. M., and A. Mogilner. 2007. Model of polarization and bistability of cell fragments. *Biophys. J.* 93:3811–3819.
60. Holmes, W. R., J. Park, …, L. Edelstein-Keshet. 2017. A mathematical model coupling polarity signaling to cell adhesion explains

diverse cell migration patterns. *PLoS Comput. Biol.* 13:10055244–e1005622.

61. Ron, J. E., P. Monzo, …, N. S. Gov. 2020. One-dimensional cell motility patterns. *Phys. Rev. Research.* 2:033237.
62. Sens, P. 2020. Stick–slip model for actin-driven cell protrusions, cell polarization, and crawling. *Proc. Natl. Acad. Sci. USA.* 117:24670–24678.
63. Zimmermann, J., M. Enculescu, and M. Falcke. 2010. Leading edge - gel coupling in lamellipodium motion. *Phys. Rev. E - Stat. Nonlinear Soft Matter Phys.* 82:051925.
64. Craig, E. M., J. Stricker, …, A. Mogilner. 2015. Model for adhesion clutch explains biphasic relationship between actin flow and traction at the cell leading edge. *Phys. Biol.* 12:035002.
65. Schreiber, C., F. J. Segerer, …, J. O. Rädler. 2016. Ring-shaped microlanes and chemical barriers as a platform for probing single-cell migration. *Sci. Rep.* 6:26858.
66. Mogilner, A., and G. Oster. 2003. Force generation by actin polymerization II: the elastic ratchet and tethered filaments. *Biophys. J.* 84:1591–1605.
67. Footer, M. J., J. W. J. Kerssemakers, …, M. Dogterom. 2007. Direct measurement of force generation by actin filament polymerization using an optical trap. *Proc. Natl. Acad. Sci. USA.* 104:2181–2186.
68. Gholami, A., J. Wilhelm, and E. Frey. 2006. Entropic forces generated by grafted semiflexible polymers. *Phys. Rev. E - Stat. Nonlinear Soft Matter Phys.* 74:041803.
69. Wilson, K., A. Lewalle, …, G. Charras. 2013. Mechanisms of leading edge protrusion in interstitial migration. *Nat. Commun.* 4:2896.
70. Guo, M., A. F. Pegoraro, …, D. A. Weitz. 2017. Cell volume change through water efflux impacts cell stiffness and stem cell fate. *Proc. Natl. Acad. Sci. USA.* 114:E8618–E8627.
71. Motahari, F., and A. E. Carlsson. 2019. Thermodynamically consistent treatment of the growth of a biopolymer in the presence of a smooth obstacle interaction potential. *Phys. Rev. E.* 100:042409.
72. Mitchison, T., and M. Kirschner. 1988. Cytoskeletal dynamics and nerve growth. *Neuron.* 1:761–772.
73. Suter, D. M., and P. Forscher. 1998. An emerging link between cytoskeletal dynamics and cell adhesion molecules in growth cone guidance. *Curr. Opin. Neurobiol.* 8:106–116.
74. Suter, D. M., and P. Forscher. 2000. Substrate–cytoskeletal coupling as a mechanism for the regulation of growth cone motility and guidance. *J. Neurobiol.* 44:97–113.
75. Jurado, C., J. R. Haserick, and J. Lee. 2005. Slipping or gripping? Fluorescent speckle microscopy in fish keratocytes reveals two different mechanisms for generating a retrograde flow of actin. *Mol. Biol. Cell.* 16:507–518.
76. Hu, K., L. Ji, …, C. M. Waterman-Storer. 2007. Differential transmission of actin motion within focal adhesions. *Science.* 315:111–115.
77. Gardel, M. L., B. Sabass, …, C. M. Waterman. 2008. Traction stress in focal adhesions correlates biphasically with actin retrograde flow speed. *J. Cell Biol.* 183:999–1005.
78. Aratyn-Schaus, Y., and M. L. Gardel. 2010. Transient frictional slip between integrin and the ECM in focal adhesions under myosin II tension. *Curr. Biol.* 20:1145–1153.
79. Li, Y., P. Bhimalapuram, and A. R. Dinner. 2010. Model for how retrograde actin flow regulates adhesion traction stresses. *J. Phys. Condens. Matter.* 22:194113.
80. Heath, J. P., and B. F. Holifield. 1993. On the mechanisms of cortical actin flow and its role in cytoskeletal organisation of fibroblasts. *Symp. Soc. Exp. Biol.* 47:35–56.
81. Vallotton, P., G. Danuser, …, A. B. Verkhovsky. 2005. Tracking retrograde flow in keratocytes: news from the front. *Mol. Biol. Cell.* 16:1223–1231.
82. Renkawitz, J., K. Schumann, …, M. Sixt. 2009. Adaptive force transmission in amoeboid cell migration. *Nat. Cell Biol.* 11:1438–1443.
83. Alexandrova, A. Y., K. Arnold, …, A. B. Verkhovsky. 2008. Comparative dynamics of retrograde actin flow and focal adhesions: formation of nascent adhesions triggers transition from fast to slow flow. *PLoS One.* 3:e3234.
84. Choquet, D., D. P. Felsenfeld, and M. P. Sheetz. 1997. Extracellular matrix rigidity causes strengthening of integrin–cytoskeleton linkages. *Cell.* 88:39–48.
85. Fournier, M. F., R. Sauser, …, A. B. Verkhovsky. 2010. Force transmission in migrating cells. *J. Cell Biol.* 188:287–297.
86. Ebeling, W. 1989. Chaos, Ordnung und Information. Urania Verlag Leipzig.
87. Popp, K., and P. Stelter. 1990. Stick-slip vibrations and chaos. *Phil. Trans. Phys. Sci. Eng.* 332:89–105.
88. Brace, W. F., and J. D. Byerlee. 1966. Stick-slip as a mechanism for earthquakes. *Science.* 153:990–992.
89. Lee, D. W., X. Banquy, and J. N. Israelachvili. 2013. Stick-slip friction and wear of articular joints. *Proc. Natl. Acad. Sci. USA.* 110:E567–E574.
90. Barnhart, E., K.-C. Lee, …, A. Mogilner. 2015. Balance between cell-substrate adhesion and myosin contraction determines the frequency of motility initiation in fish keratocytes. *Proc. Natl. Acad. Sci. USA.* 112:5045–5050.
91. Rutkowski, D. M., and D. Vavylonis. 2021. Discrete mechanical model of lamellipodial actin network implements molecular clutch mechanism and generates arcs and microspikes. *PLoS Comput. Biol.* 17:e1009506–e1009532.
92. Chan, C. E., and D. J. Odde. 2008. Traction dynamics of Filopodia on compliant substrates. *Science.* 322:1687–1691.
93. Wolgemuth, C. W. 2005. Lamellipodial contractions during crawling and spreading. *Biophys. J.* 89:1643–1649.
94. Evans, E. 2001. Probing the relation between force - lifetime - and chemistry in single molecular bonds. *Annu. Rev. Biophys. Biomol. Struct.* 30:105–128.
95. van Kampen, N. 2001. Stochastic Processes in Physics and Chemistry. North-Holland, Amsterdam.
96. Cirit, M., M. Krajcovic, …, J. M. Haugh. 2010. Stochastic model of integrin-mediated signaling and adhesion dynamics at the leading edges of migrating cells. *PLoS Comput. Biol.* 6:e1000688.
97. Weichsel, J., and U. S. Schwarz. 2010. Two competing orientation patterns explain experimentally observed anomalies in growing actin networks. *Proc. Natl. Acad. Sci. USA.* 107:6304–6309.
98. Bhalla, U. S. 2004. Signaling in small subcellular volumes. I. Stochastic and diffusion effects on individual pathways. *Biophys. J.* 87:733–744.
99. Bialek, W., and S. Setayeshgar. 2005. Physical limits to biochemical signaling. *Proc. Natl. Acad. Sci. USA.* 102:10040–10045.
100. Tsimring, L. S. 2014. Noise in biology. *Rep. Prog. Phys.* 77:026601.
101. Falcke, M. 2017. Life is change – dynamic modeling quantifies it. *Curr. Opin. Struct. Biol.* 3:iv–viii.
102. Coué, M., S. L. Brenner, …, E. D. Korn. 1987. Inhibition of actin polymerization by latrunculin A. *FEBS Lett.* 213:316–318.
103. McGrath, J. L., N. J. Eungdamrong, …, S. C. Kuo. 2003. The force-velocity relationship for the actin-based motility of Listeria monocytogenes. *Curr. Biol.* 13:329–332.
104. Koseki, K., D. Taniguchi, …, N. Watanabe. 2019. Lamellipodium tip actin barbed ends serve as a force sensor. *Gene Cell.* 24:705–718.
105. Peskin, C. S., G. M. Odell, and G. F. Oster. 1993. Cellular motions and thermal fluctuations: the Brownian ratchet. *Biophys. J.* 65:316–324.
106. Bieling, P., T. D. Li, …, R. D. Mullins. 2016. Force feedback controls motor activity and mechanical properties of self-assembling branched actin networks. *Cell.* 164:115–127.
107. Dolati, S., F. Kage, …, M. Falcke. 2018. On the relation between filament density, force generation, and protrusion rate in mesenchymal cell motility. *Mol. Biol. Cell.* 29:2674–2686.

108. Dickinson, R. B., and D. L. Purich. 2002. Clamped-filament elongation model for actin-based motors. *Biophys. J.* 82:605–617.

109. Trichet, L., O. Campàs, …, J. Plastino. 2007. VASP governs actin dynamics by modulating filament anchoring. *Biophys. J.* 92:1081–1089.

110. d'Alessandro, J., A. Barbier-Chebbah, …, B. Ladoux. 2021. Cell migration guided by long-lived spatial memory. *Nat. Commun.* 12:4118.

111. Harburger, D. S., and D. A. Calderwood. 2009. Integrin signalling at a glance. *J. Cell Sci.* 122:159–163.

112. Warner, H., B. J. Wilson, and P. T. Caswell. 2019. Control of adhesion and protrusion in cell migration by Rho GTPases. *Curr. Opin. Cell Biol.* 56:64–70.

113. Tkachenko, E., M. Sabouri-Ghomi, …, M. H. Ginsberg. 2011. Protein kinase A governs a RhoA-RhoGDI protrusion-retraction pacemaker in migrating cells. *Nat. Cell Biol.* 13:660–667.